Korean J. Chem. Eng., 39(8), 2044-2054 (2022)
DOI: 10.1007/s11814-022-1107-2

pISSN: 0256-1115
eISSN: 1975-7220

Experimental studies of bubble cutting in a lab-scale micro-structured bubble column with different liquid viscosity

Guanghui Chen, Zhongcheng Zhang, Fei Gao, Jianlong Li, and Jipeng Dong†

College of Chemical Engineering, Qingdao University of Science and Technology, Qingdao 266043, China
(*Received 6 November 2021 • Revised 28 February 2022 • Accepted 12 March 2022*)

Abstract−Bubble cutting was realized by installing a wire mesh in a micro-structured bubble column (MSBC) and studied experimentally with liquid viscosity range from 1 to 39.6 mPa·s. A non-intrusive high-speed camera method was used to determine bubble size and size distribution. The changes of gas holdup, bubble size, size distribution and Sauter mean diameter before and after cutting were systematically studied with mesh openings of 3.8 mm and 5.5 mm. Three novel bubble cutting behaviors with uniform cutting, detachment cutting and indirect cutting behavior were observed. In the presence of two wire meshes, the bubble size distribution roughly shows a Gaussian curve distribution and the peak tends to shift towards lower diameters. With increasing liquid viscosity and superficial gas velocity, the dominant peak tends to move towards higher diameters, resulting in poor mesh cutting effect. After cutting, in the case of two wire meshes, the Sauter mean diameter decreased by 33.5% and 22.2% and the gas holdup increased by 3.2-12.2% and 1.2-4.4%, respectively. For the case of 3.8 mm mesh opening, the interfacial area increased by 10-26%, which is much better than 5.5 mm mesh. The mean bubble size above the mesh will grow again and its growth rate depends on the liquid viscosity.

Keywords: Micro-structured Bubble Column, Bubble Cutting, Bubble Size Distribution, Liquid Viscosity, Wire Mesh

INTRODUCTION

As efficient multiphase contactors and reactors, bubble column reactors (BCR) have been extensively applied in chemical engineering and related fields, including chemical adsorption and biological reactions [1-5]. BCR is one of the most commonly used reactor types in gas-liquid reaction, which is mainly used in high interfacial area and intense mixing of the liquid phase is necessary [6]. Its characteristics, such as simple geometry arrangement and compactness, low operating and maintenance costs, high effective interfacial area and excellent mixing capability, are attractive in the aspect of mass and heat transfer [7]. However, in spite of their simplicity in geometrical construction, the design of BCR, the improvement of its mass transfer efficiency, scale-up and process optimization still face great difficulties [8-10]. However, coalescence, caused by the interaction between bubbles, is a common process that has a great influence on the resulting bubble size distribution. In BCRs, the pronounced coalescence between bubbles greatly impedes the increase of the gas-liquid interfacial area, which the performance of the reactor is mostly restricted by the mass transfer rate and heat removal rate [11].

Enhancing the mass transfer process to improve efficiency and economic benefit has always been the focus of multiphase flow research. The volumetric mass transfer coefficient, $k_l\alpha$, which depends on the two-phase physical properties and the operating conditions, is regarded as a key parameter to characterize the mass transfer efficiency and capacity [12]. However, mass transfer is not only related to the gas-liquid volumetric mass transfer coefficient $k_l\alpha$, but it also depends on liquid velocity, gas holdup and interfacial area [13,14]. The enhanced mass transfer process is associated with bubble coalescence and breakup, since this process creates poly-disperse bubble swarms. Li and Kang [15] found that the variation of the mass transfer coefficient has a significant crest observed for all the presented cases at a column height, which is in agreement with the trend for the occurrence frequency of bubble coalescence and breakup. Mass transfer can be promoted by the process of coalescence and breakup in the liquid phase within a certain intensity range. An effective method of installing the internals to enhance the bubble breakup process has been adopted and studied in some research [16-19].

In BCRs, generating small bubbles is perceived as an effective step to improve the heat and mass transfer rate. Cutting is a very important and commonly used method of forced bubble breaking, which cuts large bubbles into smaller ones by setting internals such as wire or screen meshes in the rising path of the bubbles [20-23]. A smaller bubble size can result in a lower rising velocity, a lesser turbulence, a greater gas holdup, a larger gas-liquid interfacial area and the rate of diffusion [24,25]. Wire meshes coated with catalyst can be introduced to cut the larger bubbles, improve the gas-liquid interfacial area and avoid adding external filtration equipment to separate the catalyst. The interaction between the wire mesh and the bubbles also enhances the interface dynamics, from which a higher surface renewal rate and local mass transfer rate could be realized [11]. In our previous work [26-28], we broke the bubble by setting up a mesh on the sieve tray and found that the mean bubble size can be significantly reduced and the gas holdup can be in-

†To whom correspondence should be addressed.
E-mail: dongjipeng0302@163.com
Copyright by The Korean Institute of Chemical Engineers.

creased after the installation of the mesh. We found that bubble cutting is an effective method to promote gas-liquid mass transfer, since bubble breakup behavior will increase the gas-liquid mass transfer area, update the phase boundary. Zhang et al. [29] investigated the influence of different screens mesh on the gas holdup and bubble rising velocity in the internal loop airlift reactor. The bubble velocity distribution is more uniform when a screen mesh is installed and higher gas holdup can be obtained. Jain et al. [11] developed a new model for bubble cutting based on the 3D discrete bubble model (3D-DBM) in a micro-structured bubble column (MSBC) and the effect of key parameters such as the mesh opening and the superficial gas velocity was preliminarily studied. The volume of fluid (VOF) model is widely used to study the phase interface. Baltussen et al. [30,31] used the VOF model combined with experimental verification to investigate the interaction between wire, wire mesh and single bubble, respectively. Sujatha et al. [32] developed a novel MSBC by using the wire mesh to overcome some drawbacks such as high coalescence rates and short gas phase residence time at high gas flowrates, which result in a greater degree of back-mixing and low interfacial area in the gas-liquid phase.

Air-water bubble columns have been extensively adopted in many bubble cutting studies. However, organic liquids are often used in industrial production and only the air-water system involved is not sufficient. The characteristics of bubble dynamics are greatly determined by the liquid parameters and the flow regime around the bubble [33]. Among the liquid parameters, viscosity μ_l and surface tension σ are two critical parameters affecting the hydrodynamics of bubbles. Kováts et al. [34] found that differences in the bubble size distribution results significantly depend on viscosity and surface tension. At present, research on bubble cutting behavior is mainly based on the air-water system [35], and there is little research on other liquid systems. Compared with water, high viscosity liquids contribute to a smaller gas holdup, larger bubble size and lower mass transfer rate. In the case of high viscosity fluid, enhanced mass transfer process should be focused, but the effects of different liquid properties on bubble cutting have not been explored in depth. Baltussen et al. [30] used a glycerol solution in their experiment to ensure that the bubbles could pass the single wire without being cut, but only the interaction between a single wire and a single bubble was taken into account. Therefore, in this work, we consider the influence of liquid viscosity under the condition that the surface tension is approximately equal. A comprehensive and multi-level perspective is essential to quantitatively describe the effects of viscosity on hydrodynamics and mass transfer behavior, which has a significant impact on the operation, optimization and scale-up of the reactors [36].

In the present work, we conducted experiments to thoroughly investigate the interaction between wire mesh and bubble cutting behavior under different liquid viscosities in an MSBC reactor. The viscosity allows to be changed by adding different concentrations of aqueous glycerol solution without affecting the surface tension of the liquid prominently. Therefore, in this paper, the effect of surface tension on bubble behavior can be ignored. In addition, the effect of different wire meshes on bubble cutting performance with different viscosity was also investigated. The bubble size, size distribution, gas holdup ε_g, the Sauter mean diameter d_{32} and interfacial area a before and after bubble cutting were analyzed in detail by a non-intrusive high-speed camera method to determine the influence of liquid viscosity on bubble cutting in BCRs.

EXPERIMENTAL SETUP

A schematic of the experimental and photography devices for bubble measurement is shown in Fig. 1. The rectangular BCR with dimensions of 120 mm width×25 mm depth×840 mm height was made of transparent plexiglass used for bubble size and bubble formation number measurement in the experiment. The rectangular structure allows easier visual observation and optical measurement than the cylindrical ones [37] and has sufficient optical accessibility under low gas fraction (3-5%) to obtain good bubble capture images for analysis [38]. At higher gas flowrate, more obvious bubble overlap occurs, and the area covered by bubble shadow is larger, which the visual observation and experimental measurement will add further uncertainty.

Aqueous glycerol solution was the liquid phase and air was used as the gas phase. Aqueous glycerol solutions of different concentrations were used to study the effect of viscosity on bubble cutting, since the surface tension used in this experiment was similar [39]. The addition of different doses of glycerol solution to water allows an increment in the viscosity of the solution with little change in liquid surface tension. The surface tension of glycerol aqueous solution with different concentrations is approximately the same, while the viscosity changes significantly. The variation of liquid surface tension is very little, resulting in very small changes in bubble size, cutting process and gas holdup. In this work, the influence of surface tension on the measured results in the experiment was not considered. The physical properties of the liquid phase are listed in Table 1. As shown in Fig. 2, the internals used in this work were wire mesh. The wire mesh was fixed 150 mm above the gas inlet for the experiments. Two types of mesh used in the experiment have similar wire diameters (0.5 mm and 0.7 mm) and different

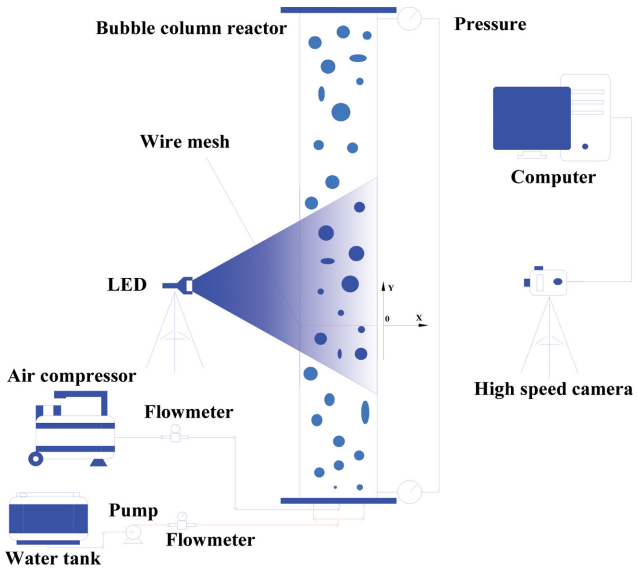


Fig. 1. Experimental devices for bubble measurement.

Table 1. Liquid phase physical properties at 25 °C

Glycerol solutions wt%	Viscosity μ_l (mPa·s)	Density ρ_l (kg/m^3)	Surface tension σ (N/m)
0.0	1	1,000	0.0725
54.9	7.9	1,124	0.0636
69.9	20.1	1,140	0.0632
76.6	39.6	1,184	0.0621

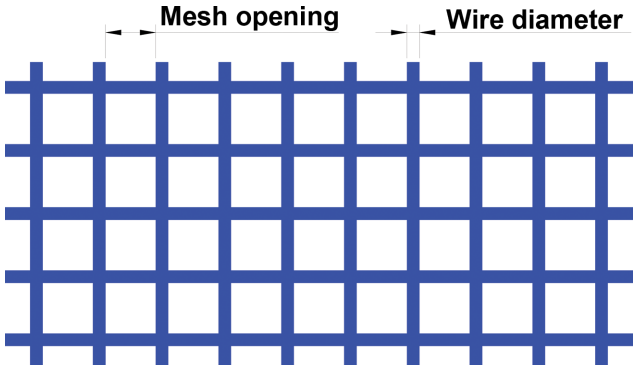


Fig. 2. Structure of the wire mesh.

mesh openings (3.8 mm and 5.5 mm). In this work, the experiment was operated under a homogeneous bubble flow regime.

MEASUREMENT METHODS

1. Gas Holdup Measurement

In this work, the pressure drop method was used to measure the gas holdup ε_g by a differential pressure transmitter at a height of 600 mm. The relationship between the pressure drop and gas holdup can be calculated according to the following equation:

$$\Delta P = \rho_l g h (1 - \varepsilon_g) \quad (1)$$

In addition, the gas holdup also can be calculated as follows:



Fig. 3. Calibrate the camera's focus position.

$$\varepsilon_g = (\Delta P_1 - \Delta P_2)/\Delta P_1 \quad (2)$$

2. Bubble Size and Size Distribution Measurement

A transparent scale was used to calibrate the camera's focus position (see Fig. 3) and length of the unit pixel was determined (see

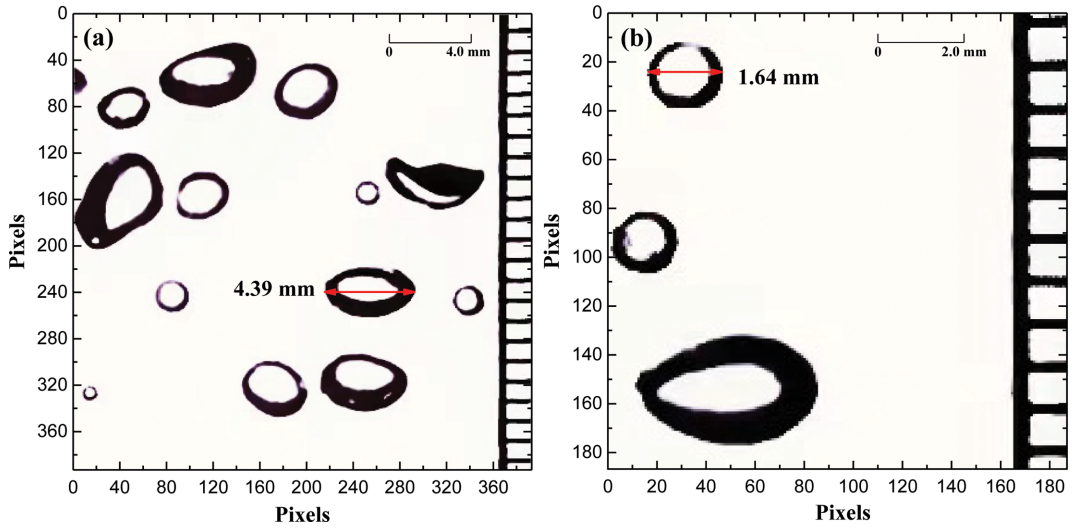


Fig. 4. Measure the size of the bubble with different spatial resolutions. Left: 0.057 mm/pixel, right: 0.055 mm/pixel.

Fig. 4). The shooting positions in the vertical direction were located at the wire mesh, which were monitored by moving the high-speed camera and LED light to the corresponding height.

In previous studies, only a constant bubble diameter was used and either empirical correlation or theoretical analysis was calculated [40]. However, the image of the bubble recorded by a high-speed camera is two-dimensional and the deformation of bubbles should also be taken into account. It is difficult to obtain regular round bubbles. Therefore, the bubble equivalent diameter d_{eq} was introduced to replace the diameter of each deformed bubble in the field of engineering due to its simplicity and practicability [41,42], which can be expressed as:

$$d_{eq} = 2\sqrt{(A_b/\pi)} \tag{3}$$

Bubble Sauter mean diameter d_{32} determines the interfacial mass transfer capacity in a MSBC because the interfacial area for gas-liquid two-phase greatly depends on d_{32}. The Sauter mean diameter d_{32} can be calculated from the bubble equivalent diameter d_{eq} [43]:

$$d_{32} = \Sigma_{i=1}^{n} d_{eq,i}^{3} / \Sigma_{i=1}^{n} d_{eq,i}^{2} \tag{4}$$

The gas-liquid interfacial area *a* can be estimated by the Sauter mean diameter and gas holdup obtained from the experimental data [44,45]:

$$a = 6\varepsilon_g / d_{32} \tag{5}$$

The probability density function (PDF) for a particular bubble diameter $d_{eq,i}$ class is calculated from the number of bubbles and equivalent bubble diameter can be defined as:

$$PDF_{d_{eq,i}} = n_{d_{eq}} / \Sigma_{d_{eq,min}}^{d_{eq,max}} n_{d_{eq,i}} \tag{6}$$

RESULTS AND DISCUSSION

1. Visual Observation

We directly analyzed the bubble image captured by a high-speed camera operated at 50 Hz. We can see from visual observation in Fig. 5, in the case of 1 mPa·s solution, bubble size mainly ranges from 3.5 to 5.5 mm without wire mesh (Fig. 5(a)). The bubble size varies within a small range, since bubble coalescence and breakup are suppressed to the greatest extent in the homogeneous regime. It is well known that the interaction between bubbles has a great impact on bubble size distribution. Another interaction, between the bubbles and the wire mesh, also has a significant effect on the resulting bubble size and its distribution. As shown in Fig. 5(b) and Fig. 5(c), the bubble size is significantly reduced, the bubble size distribution becomes wider and the number of bubbles increases dramatically in the MSBC equipped with a wire mesh. In addition, the bubbles are extremely irregular, which are mostly angular. These heavily deformed bubbles can be broken into smaller bubbles by an external force such as fluid shear force or coalesce with surrounding bubbles to form larger bubbles.

The interaction between the bubbles and the wire mesh is more complex than that of a single wire. Three novel bubble cutting behaviors were observed in this work. The bubble shape, besides the diameter and rising velocity of bubbles which affect the bubble cutting behavior, also is a non-negligible factor. Bubbles of different shapes with the same equivalent diameter that have a larger projected area in the vertical direction with the mesh are more likely to be in a position to interact with more wires and be cut into multiple small daughter bubbles. The experimental capture image of large bubbles being cut into multiple small bubbles by wire mesh is shown in Fig. 6. The two irregular bubbles close to the wire mesh have a maximum chord length of about 5.5 mm, and can interact with the two wires and be cut into six sub-bubbles of similar size. This cutting behavior may also be called uniform cutting or equal-diameter cutting behavior.

The part of the bubble that passes through the mesh has been cut up into daughter bubbles (Fig. 7(b)), but as the cutting process continues, the daughter bubbles immediately coalesce into a large daughter bubble (Fig. 7(c)) due to the small spacing of bubbles before the cutting is finished. The bubbles formed by the re-coalescence

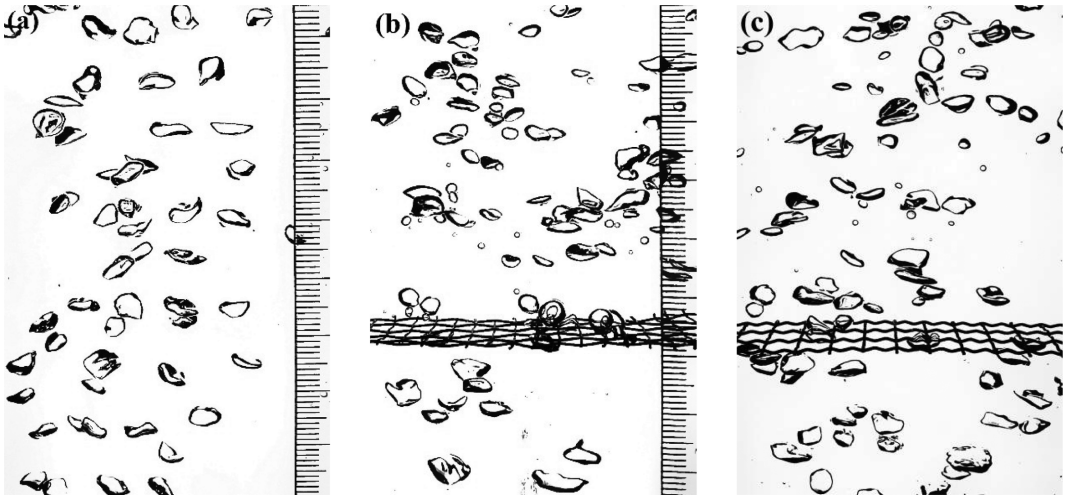


Fig. 5. Bubble cutting behavior at a superficial gas velocity of 3.5 mm/s in 1 mPa·s solution. Left: without mesh, middle: with a 3.8 mm mesh opening, right: with a 5.5 mm mesh opening.

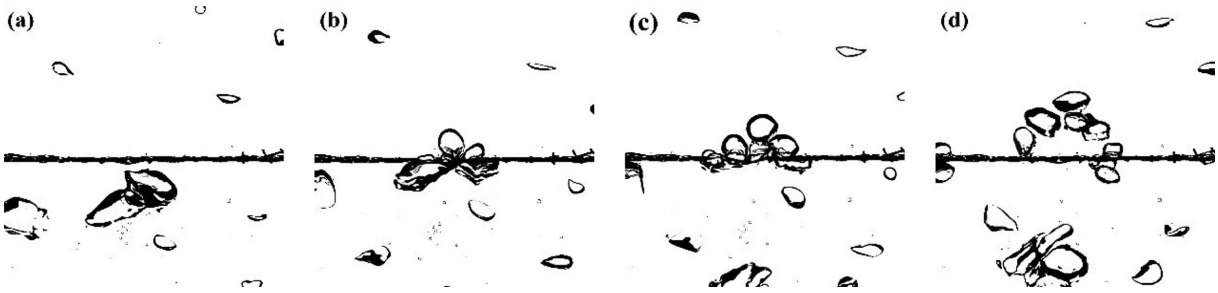


Fig. 6. Bubble uniform cutting behavior.

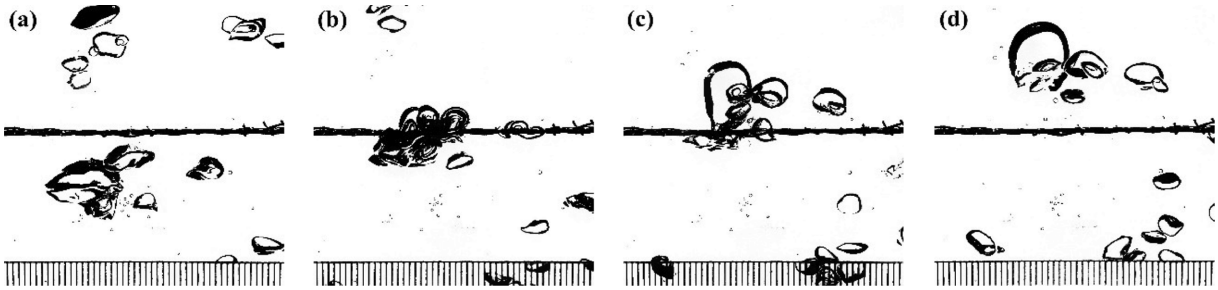


Fig. 7. Bubble detachment cutting behavior.

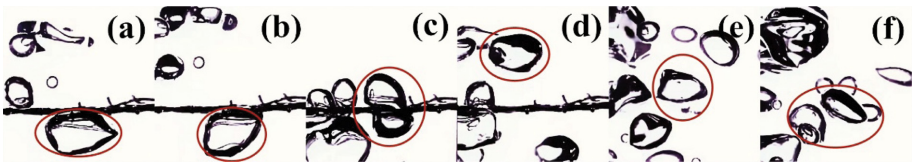


Fig. 8. Bubble indirect cutting behavior: bubble breakage caused by the bubble surface instability.

have greater buoyancy and rising velocity, and will lead to preferentially separating from the mother bubble (Fig. 7(d)), while the rest of the mother bubble may be cut or through the mesh. The bubbles produced by this cutting behavior vary in size. The cutting behavior described above is called detachment cutting behavior or non-uniform cutting behavior.

Without the influence of other bubbles, most of the trapped lemon-shaped bubbles will deform in place (Fig. 8(a) and Fig. 8(b)). The bubbles are elongated in the vertical direction as they pass through the mesh, forming a peanut-shape (Fig. 8(c)). Another bubble cutting behavior is illustrated in Fig. 8. The most intuitive manifestation of this cutting behavior is that the bubble breakup occurs after passing through the mesh. When the bubbles pass through the mesh without being cut (Fig. 8(c)), the mesh will increase the instability at the larger daughter bubble surface, leading to the sharp fluctuation of the bubble surface, which contributes to bubble breakup in the rising process. The above phenomenon occurs more frequently in the liquid phase with lower viscosity. As the viscosity increases, the fluctuation of the bubble surface caused by the mesh or collision will be greatly reduced. This pseudo-contact bubble cutting phenomenon is called indirect cutting behavior.

Fig. 9 shows the bubble cutting behavior in three glycerol solutions with different viscosities. As the viscosity increases, the bubbles become rounder. Combined with the change in the size and shape of the bubbles, the bubbles within a certain size range are observed will get stuck underneath provisionally when interacting with the mesh, especially when interacting with the intersections of the wire. This phenomenon can be noticed underneath the wire mesh when the bubbles are small or the mesh spacing is small. Increase the viscosity, and this behavior becomes more pronounced, but gas pocket cannot be observed below the wire mesh in the present work. The increase in viscosity also affects the bubble rising velocity. In all cases, a distinct experimental phenomenon has been observed that the bubble first decelerates as the bubble approaches the wire mesh. After, the mesh gradually accelerates the rise. The deceleration mechanism can be summarized as: (1) the presence of the mesh causes local vortices below and disturbs the normal development of the bubble rising path; (2) the surrounding bubbles will increase the local drag coefficient, especially in the viscous and distorted bubbles [46]. Increasing the superficial gas velocity directly increases the bubble's initial velocity; thus, the bubbles still maintain a large kinetic energy when the bubble starts passing through the mesh, and will not stop underneath the mesh due to kinetic energy depletion. In addition, we found that for smaller bubbles (≤1.0 mm), they would be trapped and difficult to escape under the influence of eddy currents below the wire mesh. This greatly increases the residence time of the small bubbles. In the field of micro bubble research, the intrusion effect of wire mesh

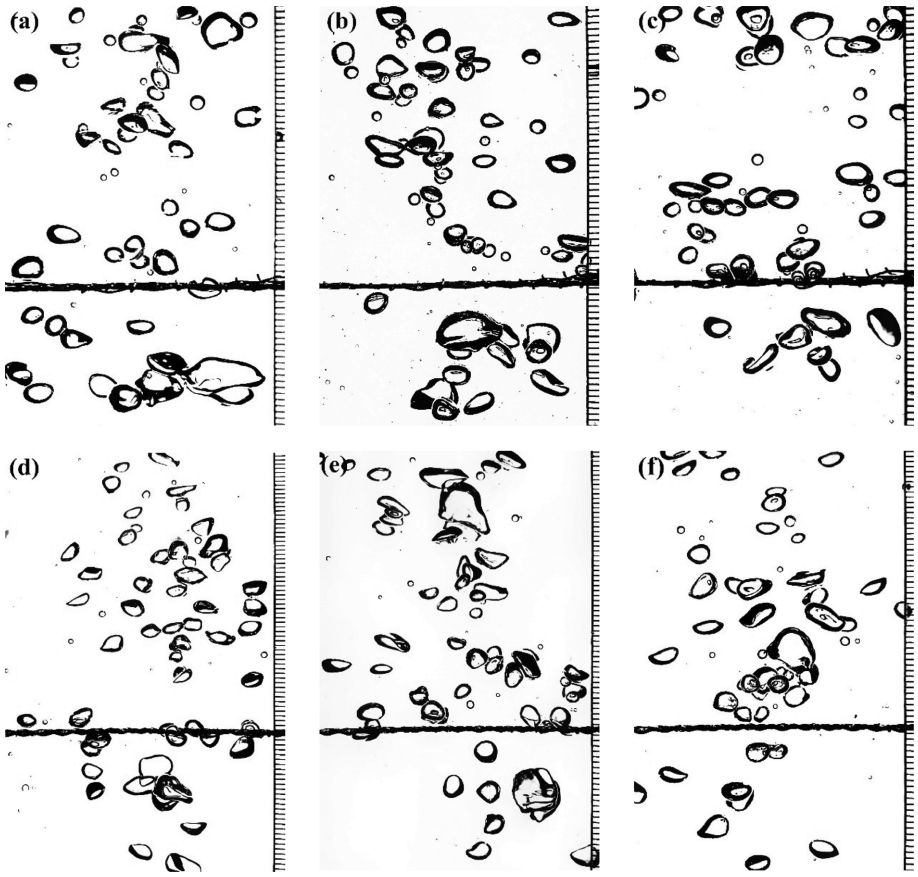


Fig. 9. Bubble cutting behavior at a superficial gas velocity of 3.5 mm/s under different liquid viscosities. The upper row shows the with a 3.8 mm mesh opening while the lower row shows the with a 5.5 mm mesh opening. From left to right, they represent the case of 7.9 mPa·s, 20.1 mPa·s and 39.6 mPa·s solution, respectively.

also increases the turbulence intensity near the wire mesh. Smaller bubbles are more likely to be trapped and the gas-liquid mixing time is prolonged, which greatly improves the mass transfer process of gas-liquid two-phase flow.

2. Effect of Viscosity on Bubble Cutting Behavior

Fig. 10 shows the bubble size distribution under different liquid viscosities with and without wire mesh. With increasing viscosity and superficial gas velocity U_{sg} (Figs. 10(a), 10(d) and 10(g)), results in the bubble size distribution range and size peak value shifting to the right entirety, and the mean bubble diameter growing by degrees. However, different from the results presented in literature, Kováts et al. [34], the bubble size distribution width was almost unchanged in this work, which may be related to the reactor size and the flow regime. The change in the bubble size distribution was marginal when the liquid viscosity was increased from 1 to 7.9 mPa·s. But it increased when the liquid viscosity was further increased to 20.1 and 39.6 mPa·s, respectively, suggesting that the prevailing effect of changing the liquid viscosity in BCRs changes the bubble coalescence and breakup rate. In the low liquid viscosity range (≤1 mPa·s), with the increase of superficial gas velocity, the change of bubble size and its distribution is small, and the proportion of bubbles with size less than 4.3 mm is almost unchanged. The small change in bubble size distribution can be thought to be caused by the change in inlet velocity; the bubble size and its distribution were almost independent of the liquid viscosity, indicating with the decrease of viscosity that the coalescence rate of bubbles is inhibited and the frequency of bubble breakage does not increase greatly. While with increasing liquid viscosity (≥7.9 mPa·s), the influence of liquid viscosity on bubble behavior is reflected in that it enhances bubble coalescence rate and inhibits breakup rate.

As shown in the second and third columns in Fig. 10, a significant change is noticeable in the bubble size distribution between the measurements with and without wire mesh, and the increase of viscosity has a great influence on bubble size distribution. Compared to the presence of no wire mesh (the first column in Fig. 10), the bubble size distribution shifts to the left and the peak tends to shift towards lower diameters. Before adding the mesh, the bubble size distribution presents a pseudo-Gaussian curve distribution with most bubbles' size range of about 4.5 mm in 1 and 7.9 mPa·s solutions, and a range of about 5.0 mm in other cases. In the presence of the wire mesh, a roughly Gaussian size distribution is still obtained with most bubbles ranging from 3.0 to 5.0 mm, with only one dominant peak that tends to shift towards higher diameters with the increase of liquid viscosity. After inserting 3.8 mm mesh opening, most bubble size in 4.5 mm below, while 5.5 mm wire mesh most bubbles in 6.0 mm below. The larger mesh opening restricts the wire mesh for the rising bubble cutting behavior, so the former has a better bubble cutting ability.

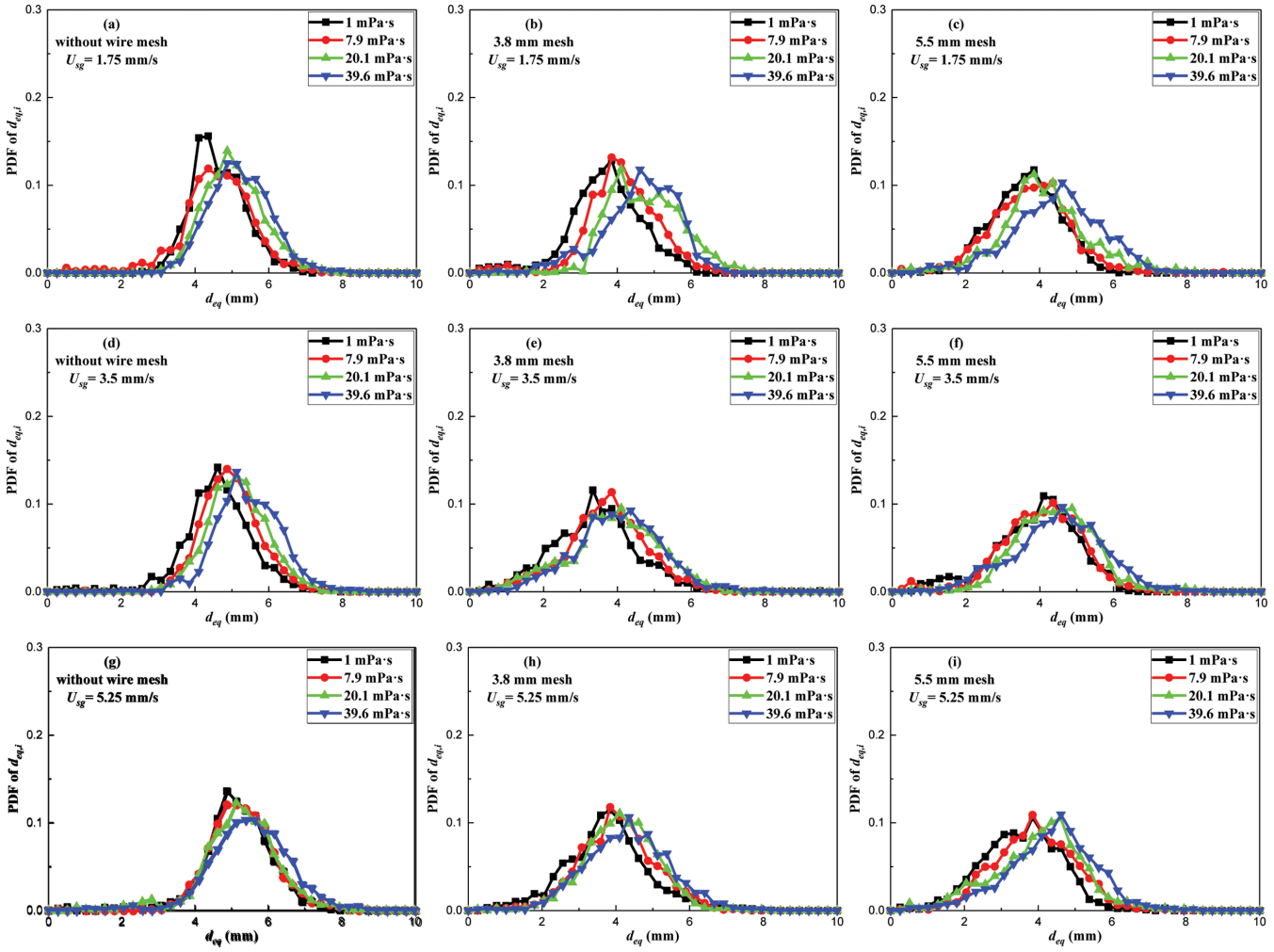


Fig. 10. Bubble size distribution. From left to right: with and without wire mesh. From top to bottom: the superficial gas velocity increases gradually.

The peak shifts towards lower diameters because the bubbles are cut by the wire mesh, while shifts towards higher diameters are due to the increased viscosity exerting an adverse influence on bubble cutting performance. Two reasons account for this adverse effect: (1) viscosity is conducive to maintaining the stability of the bubble surface, which greatly reduces the fluctuation of bubble surface caused by the interaction between bubbles or between bubbles and mesh, and even the bubble excessively elongated in the vertical direction will not break easily (see Fig. 8); (2) bubbles in high viscosity fluids are rounder, and round bubbles are not conducive to bubble cutting (see Section 4.1), resulting in bubbles more likely to pass through the wire mesh by severe deformation, especially in high viscosity fluids. The 3.8 mm mesh opening can better determine the bubble cutting effect than the wire diameter, which confirms the observation results.

3. Effect of Wire Mesh on Sauter Mean Diameter d_{32}

Fig. 11 and Fig. 12 show the comparison of the Sauter mean diameter d_{32} with and without wire mesh at a superficial gas velocity of 3.5 mm/s. The vertical black dashed line represents the location of the wire mesh. The horizontal black solid and short dashed lines (left and right) represent the average value of the Sauter mean diameter with no wire mesh, before and after bubble cutting within the vertical distance from the wire −120 mm to 120 mm, respectively. It can be seen that the Sauter mean diameter increases with liquid viscosity, both before and after cutting. In absence of a wire mesh and before the bubble interacts with the wire mesh (black dots), the Sauter mean diameter keeps on slightly increasing with height first, and stops increasing above 150 mm, which indicates that the bubble size distribution has become independent of the vertical height of the column and the bubble coalescence and breakup maintain a dynamic equilibrium state in the bubble flow. In the presence of the wire mesh, the Sauter mean diameter experiences a phase of significant decrease within 30 mm above the wire mesh. The bubbles that are successfully cut by the mesh are smaller and more numerous. In the case of 3.8 mm and 5.5 mm mesh openings, the Sauter mean diameter after cutting is approximately 33.5% and 22.2% less than that before cutting, respectively. The Sauter mean diameter gradually increases when the vertical distance to the mesh is more than 40 mm. To avoid the undesirable effects caused by re-coalescence for industrial operation, a

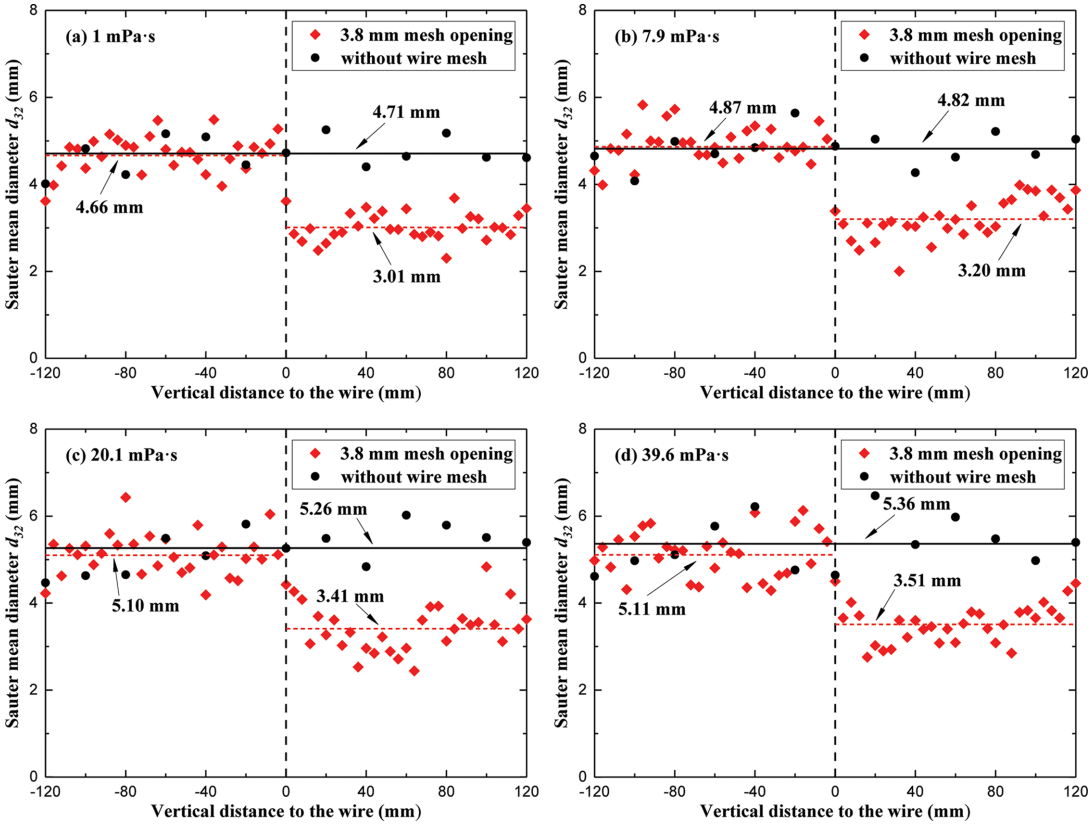


Fig. 11. Sauter mean diameter d_{32} as a function of column height with a 3.8 mm mesh opening at a superficial gas velocity of 3.5 mm/s.

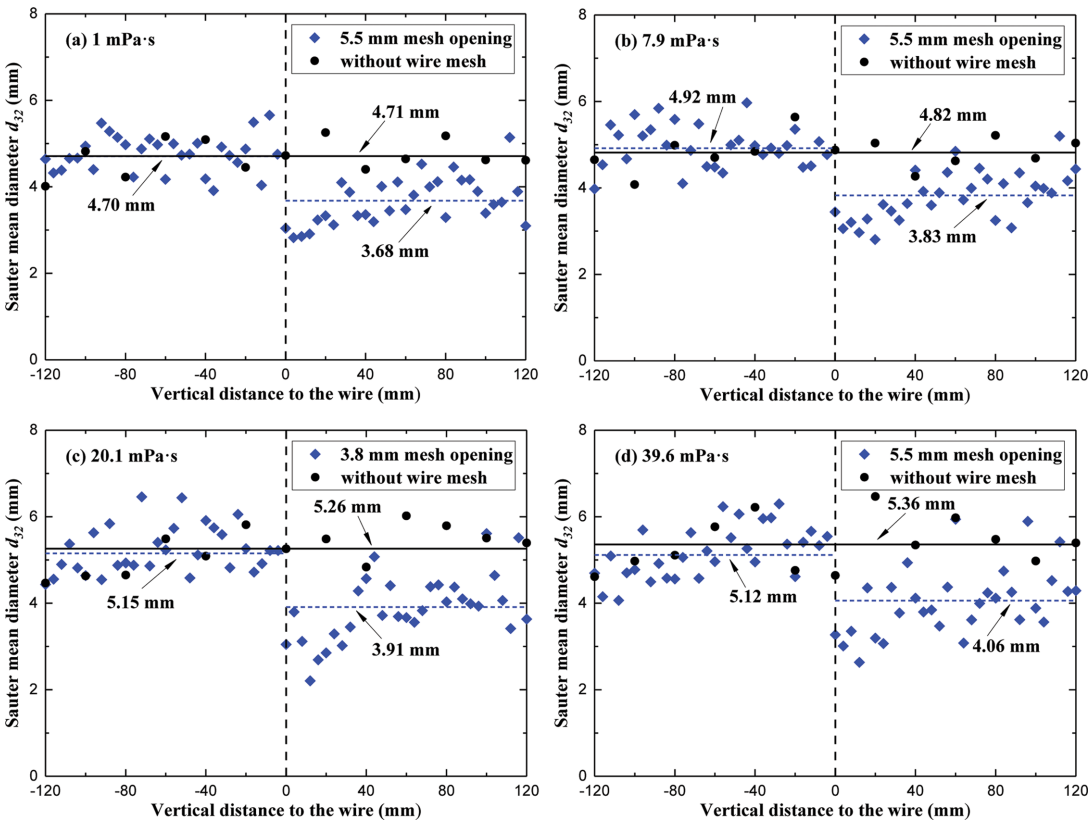


Fig. 12. Sauter mean diameter d_{32} as a function of column height with a 5.5 mm mesh opening at a superficial gas velocity of 3.5 mm/s.

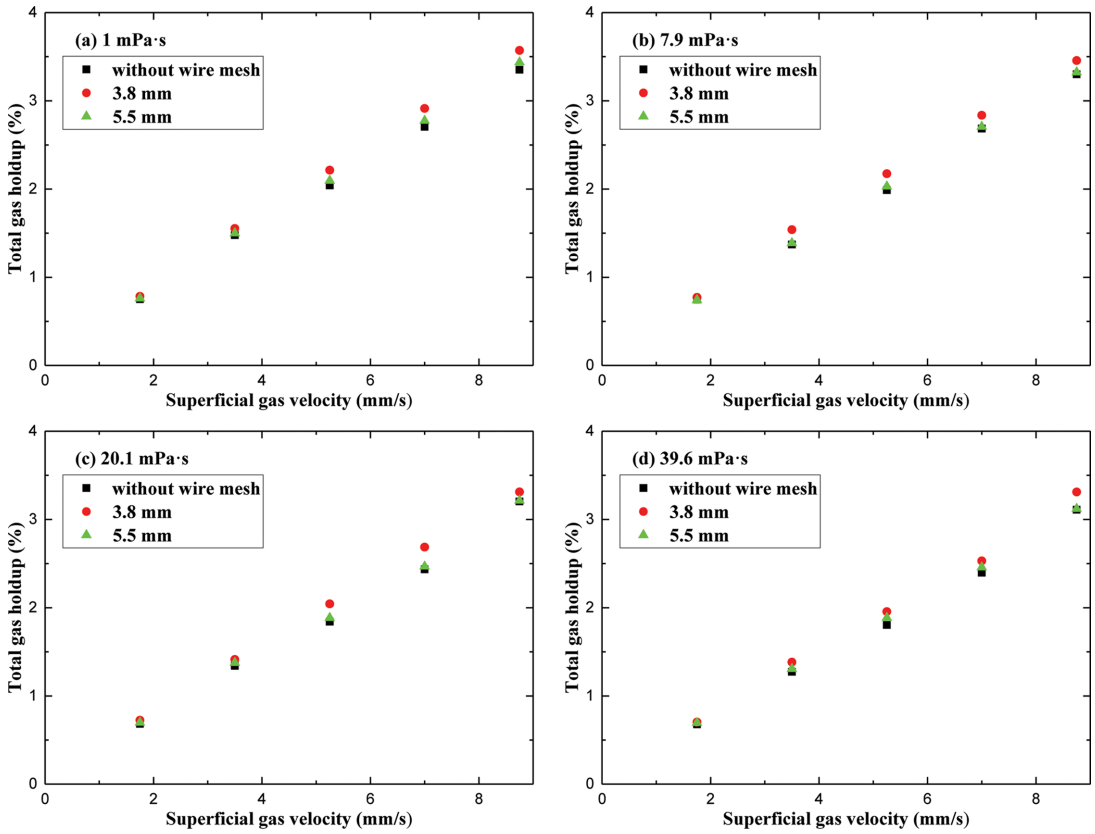


Fig. 13. Total gas holdup versus superficial gas velocity at different viscosities with and without wire mesh.

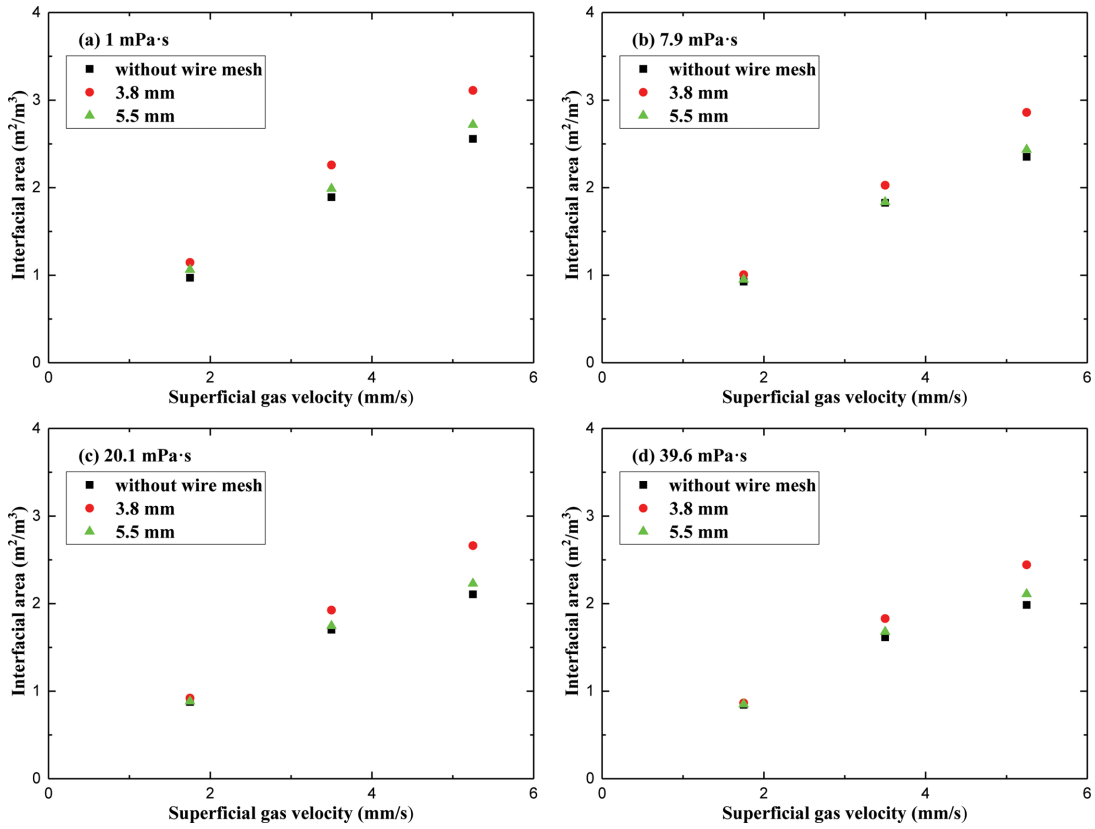


Fig. 14. Interfacial area versus the superficial gas velocity for different wire mesh openings.

method can be adopted by the use of multiple wire mesh inside the MSBC, and the bubbles are cut when growing in size again. Though the comparison can be more intuitive to find that the mesh with 3.8 mm opening in the bubble cutting effect is better than 5.5 mm.

4. Gas-holdup and Gas-liquid Interfacial Area

The gas holdup is one of the most important parameters characterizing the fluid dynamics of bubbles. Both Wilkinson et al. [47] and Kojima et al. [48] concluded that the gas holdup was directly proportional to the mass transfer coefficient. The interfacial area concentration, which is a function of Sauter mean diameter and gas holdup, is directly related to the gas-liquid mass transfer area and has a strong impact on the heat and mass transfer performance in BCRs. As can be seen in Fig. 13, the gas holdup slightly increases in the presence of the wire mesh. In the case of 3.8 mm mesh opening, the gas holdup increased by 3.2-12.2%. But, the mesh with 5.5 mm mesh opening contributes to a lower gas holdup growth rate, which only increased by 1.2-4.4%. In all cases, no significant change in gas holdup was measured as superficial gas velocity increased with addition of 7.9 mPa·s solution (Fig. 13(b)) compared to 1 mPa·s solution (Fig. 13(a)). However, a decrease in gas holdup was found with further increases in viscosity. The gas holdup for 3.8 mm mesh opening is significantly higher in comparison with no wire mesh and 5.5 mm mesh opening, and the difference increases with the superficial gas velocity. We detected that 3.8 mm mesh opening has better cutting performance than 5.5 mm mesh opening, and the significant reduction in bubble size increases the bubble residence time. The poor cutting performance for 5.5 mm opening mesh makes the change of gas holdup a little different from that without wire mesh.

A larger interfacial area than the cases with no wire mesh and 5.5 mm mesh opening was also obtained from 3.8 mm mesh opening as shown in Fig. 14, because 3.8 mm mesh opening has a larger gas holdup and a smaller Sauter mean diameter. For the case of 3.8 mm mesh opening, increasing the gas velocity increases the interfacial area by 18-21.7% in 1 mPa·s solution (Fig. 14(a)). However, increasing viscosity has no obvious effect on increasing the gas-liquid interfacial area at low superficial gas velocity, but further increasing the superficial gas velocity will greatly improve the growth rate of the interfacial area, which increases by 10% to 26%, indicating that increasing gas velocity can effectively increase the gas-liquid mass transfer area for a system with high viscosity. But, there is a little improvement in interfacial area at high liquid viscosity for 5.5 mm mesh opening compared with no wire mesh, which only increased by 0.44-6.32%.

CONCLUSIONS

The bubble size and size distribution have a great effect on the bubble rising velocity, residence time, gas holdup and interfacial area, thus affecting the overall performance of the gas-liquid flow system. In this work, experimental studies of bubble cutting were carried out in an MSBC with different liquid viscosities. The bubble shape and cutting behavior were analyzed by visual observation of the captured bubble images. The bubble size, size distribution, Sauter mean diameter, gas holdup and gas-liquid interfacial area were studied by a non-intrusive high-speed camera method. During the experiment, three bubble cutting behaviors were observed: uniform cutting, detachment cutting and indirect cutting. The uniform cutting produces multiple sub-bubbles of similar size. When the size difference of sub-bubbles after cutting is large, detachment cutting usually occurs. Indirect cutting behavior is mainly caused by the instability of large bubbles. In addition, the increase in viscosity makes the bubbles more rounded and likely to be stretched without breaking.

With the increase of viscosity, the bubble size distribution range and size peak value shift to the higher diameters and the mean bubble diameter increases in all cases. The increase in viscosity increases the coalescence rate of bubbles and the stability of bubbles (decreases the bubble breakup rate), and the average diameter of bubbles increases. In the presence of the wire mesh, the bubble size distribution presents roughly Gaussian curve distribution and shifts to the left, and the peak tends to shift towards lower diameters due to the bubbles being cut. The average of the Sauter mean diameter of 3.8 mm mesh opening decreases by 33.5% compared with that before cutting, while 5.5 mm mesh opening decreases by 22.2%. This means that a wire mesh with 3.8 mm mesh opening has better cutting performance. The larger mesh opening (5.5 mm) allows larger bubbles to pass through without being cut, which significantly increases the average size of the bubble after cutting. An increase in liquid viscosity reduces the wire mesh's bubble cutting performance. Compared to a mesh with 5.5 mm mesh opening, the 3.8 mm mesh opening has the most obvious effect on the increase of gas holdup and gas-liquid interfacial area, and the gas holdup increases by 3.2-12.2% and the gas-liquid interfacial area increases by 10-26%. In the experiment, micro bubbles (≤1.0 mm) were easily disturbed by fluid flow and trapped by eddy currents, which was caused by the local liquid reflux under the wire mesh insertion. This greatly increases the residence time of bubbles and is conducive to the mass transfer process between gas and liquid phases.

In the future research work, researchers can start from the macro perspective of the whole dynamic process of bubble movement, conduct detailed research on each movement behavior of bubble movement, and gradually explore the influence of improvement of each bubble behavior on the overall process.

ACKNOWLEDGEMENTS

This work was supported by the Natural Science Foundation of Shandong Province [No. ZR2018BB071], Qingdao Science and Technology Plan Application Foundation Research Project [No. 19-6-2-28-cg] and Key Research and Development Project of Shandong Province [No. 2019GSF109038]. The authors declare no conflict of interest.

NOMENCLATURE

a : gas-liquid interfacial area [m^2/m^3]
A_b : projected area [m]
d_{eq} : bubble equivalent diameter [m]
d_{32} : Sauter mean diameter [m]

g : gravitational acceleration [m/s^2]
h : distance between the pressure ports [m]
$k_l\alpha$: volumetric mass transfer coefficient [1/s]
n : number of bubbles
P : pressure [Pa]
P_1 : pressure without gas injection [Pa]
P_2 : pressures with gas injection [Pa]
U_{sg} : superficial gas velocity [m/s]
wt% : mass percent [-]

Greek letters

ε_g : gas holdup [-]
μ_l : viscosity [Pa·s]
ρ_l : density [kg/m^3]
σ : surface tension [N/m]

Abbreviations

BCR : bubble column reactor
DBM : discrete bubble model
MSBC : micro-structured bubble column
PDF : probability density function
VOF : volume of fluid

REFERENCES

1. H. Im, J. Park and J. W. Lee, *Korean J. Chem. Eng.*, **36**, 1680 (2019).
2. J. D. Liu, P. Zhou, L. Liu, S. Chen, Y. P. Song and H. J. Yan, *Chem. Eng. Sci.*, **230**, 116218 (2021).
3. L. Zhao, M. Lv, Z. Tang, T. Tang, Y. Shan, Z. Pan and Y. Sun, *Chem. Eng. J.*, **354**, 304 (2018).
4. Y. T. Shah, B. G. Kelkar, S. P. Godbole and W. D. Deckwer, *AIChE J.*, **28**, 353 (1982).
5. A. Fadili and A. H. Essadki, *Korean J. Chem. Eng.*, **38**, 924 (2021).
6. R. Kipping, H. Kyk and U. Hampel, *Chem. Eng. Sci.*, **229**, 116056 (2021).
7. A. M. Hissanaga, N. Padoin and E. E. Paladino, *Chem. Eng. Sci.*, **218**, 115531 (2019).
8. C. Leonard, J. H. Ferrasse, O. Boutin and S. Lefevre, *Chem. Eng. Res. Des.*, **100**, 391 (2015).
9. P. Rollbusch, M. Bothe, M. Becker, M. Ludwig, M. Grünewald, M. Schlüter and R. Franke, *Chem. Eng. Sci.*, **126**, 660 (2015).
10. X. F. Liang, H. Pan, Y. Su and Z. H. Luo, *Chem. Eng. Res. Des.*, **112**, 88 (2016).
11. D. Jain, Y. M. Lau, J. A. M. Kuipers and N. G. Deen, *Chem. Eng. Sci.*, **100**, 496 (2013).
12. S. S. Deshpande, K. Kar, J. Pressler, I. Tebeka, B. Martins, D. Rosenfeld and J. Biggs, *Chem. Eng. Sci.*, **205**, 350 (2019).
13. W. Kracht, G. Vallebuona and A. Casali, *Miner. Eng.*, **18**, 1067 (2005).
14. J. Q. Chen and C. S. Brooks, *Chem. Eng. Sci.*, **234**, 116435 (2021).
15. L. R. Li and Y. T. Kang, *J. CO_2 Util.*, **39**, 101170 (2020).
16. A. A. Youssef, M. H. Al-Dahhan and M. P. Dudukovic, *Int. J. Chem. Reactor. Eng.*, **11**, 169 (2013).
17. X. P. Guan, Q. S. Xu, N. Yang and K. D. P. Nigam, *Chem. Eng. Sci.*, **240**, 116674 (2021).
18. X. Xu, J. J Wang, Q. Yang, L. Wang, H. Lu, H. L. Liu and H. L. Wang, *Chin. J. Chem. Eng.*, **28**, 2968 (2020).
19. G. H. Chen, H. T. Zhu, X. L. Guo, W. W. Wang and J. L. Li, *CIESC J.*, **68**, 4633 (2017).
20. M. S. Lavasani, R. Rahimi and M. Zivdar, *Chem. Eng. Process.*, **129**, 162 (2018).
21. H. R. Mortaheb, H. Kosuge and K. Asano, *Chem. Eng. J.*, **88**, 59 (2002).
22. H. Zhao, L. Li, J. Jin and Q. Li, *Chem. Eng. Res. Des.*, **129**, 55 (2018).
23. D. Jain, J. A. M. Kuipes and N. G. Deen, *Chem. Eng. Sci.*, **137**, 685 (2015).
24. M. Opletal, P. Novotný, V. Linek, T. Moucha and M. Kordač, *Chem. Eng. J.*, **353**, 436 (2018).
25. M. Ide, H. Uchiyama and T. Ishikura, *Chem. Eng. Sci.*, **56**, 6225 (2001).
26. W. W. Wang, S. Y. Li and J. L. Li, *Ind. Eng. Chem. Res.*, **51**, 7067 (2012).
27. X. Li, W. W. Wang, P. Zhang, J. L. Li and G. H. Chen, *Roy Soc Open Sci.*, **6**, 190136 (2019).
28. G. H. Chen, H. T. Zhu, X. L. Guo, W. W. Wang and J. L. Li, *CIESC J.*, **68**, 4633 (2017).
29. X. Zhang, K. Guo, W. Qi and T. Zhang, *Can. J. Chem. Eng.*, **95**, 1202 (2016).
30. M. W. Baltussen, Q. I. E. Segers, J. A. M. Kuipes and N. G. Deen, *Chem. Eng. Sci.*, **157**, 138 (2017).
31. M. W. Baltussen, J. A. M. Kuipers and N. G. Deen, *Chem. Eng. Sci.*, **165**, 25 (2017).
32. K. T. Sujatha, B. G. J. Meeusen, J. A. M. Kuipes and N. G. Deen, *Chem. Eng. Sci.*, **130**, 18 (2015).
33. W. Zhang, J. F. Wang, B. Li, K. Yu, D. B. Wang, P. Yongphet, H. J. Xu and J. Yao, *Chem. Eng. J.*, **417**, 127982 (2021).
34. P. Kováts, D. Thévenin and K. Zähringer, *Int. J. Multiphas Flow*, **123**, 103174 (2020).
35. K. T. Sujatha, D. Jain, S. Kamath, J. A. M. Kuipes and N. G. Deen, *Chem. Eng. Sci.*, **169**, 225 (2017).
36. C. Xing, T. F. Wang and J. F. Wang, *Chem. Eng. Sci.*, **95**, 313 (2013).
37. A. Barati-Harooni and M. Jamialahmadi, *Int. J. Multiphas Flow*, **139**, 103674 (2021).
38. C. Muilwijk and H. E. A. Van den Akker, *Int. J. Multiphas Flow*, **137**, 103498 (2021).
39. H. H. Zhang, K. Y. Guo, Y. L. Wang, A. Sayyar and T. F. Wang, *Int. J. Heat. Mass. Tran.*, **161**, 120229 (2020).
40. S. W. Hu and X. H. Liu, *Chem. Eng. J.*, **413**, 127503 (2021).
41. G. Z. Xu, Z. N. Sun and X. T. Zhang, *Ann. Nucl. Energy*, **151**, 107905 (2021).
42. X. Xu, H. Zhou, S. Jing, W. J. Lan and S. W. Li, *Chem. Eng. Sci.*, **201**, 349 (2019).
43. M. Ostadrahimi, S. Farrokhpay, K. Gharibi and A. Dehghani, *Colloids Surf. A.*, **594**, 124672 (2020).
44. X. H. Zhou, Y. L. Ma, M. Y. Liu and Y. Zhang, *Powder Technol.*, **362**, 57 (2020).
45. G. Grund, A. Schumpe and W.-D. Deckwer, *Chem. Eng. Sci.*, **47**, 3509 (1992).
46. X. P. Guan and N. Yang, *Chem. Eng. Sci.*, **243**, 116758 (2021).
47. P. M. Wilkinson, H. Haringa and L. L. V. Dierendonck, *Chem. Eng. Sci.*, **49**, 1417 (1994).
48. H. Kojima, J. Sawai and H. Suzuki, *Chem. Eng. Sci.*, **52**, 4111 (1997).